Iraqi Journal for Computer Science and Mathematics

Volume 6 | Issue 1 Article 14

2025

Image denoising using smooth total variation function for 5G enhanced mobile broadband transmission system

Shehab Ahmed Ibrahem
Computer Science Department/University of Kirkuk, Kirkuk, Iraq, mullaiq@uokirkuk.edu.iq

Walled Khalid Abdulwahab
Computer Science Department/University of Kirkuk, Kirkuk, Iraq, walled.khalid@uokirkuk.edu.iq

Moceheb Lazam Shuwandy
Computer Science Department/Tikrit University, Tikrit, Iraq, moceheb@tu.edu.iq

Recommended Citation

Ibrahem, Shehab Ahmed; Abdulwahab, Walled Khalid; and Shuwandy, Moceheb Lazam (2025) "Image denoising using smooth total variation function for 5G enhanced mobile broadband transmission system," *Iraqi Journal for Computer Science and Mathematics*: Vol. 6: Iss. 1, Article 14.
DOI: https://doi.org/10.52866/2788-7421.1244
Available at: https://ijcsm.researchcommons.org/ijcsm/vol6/iss1/14

IRAQI JOURNAL FOR COMPUTER SCIENCE AND MATHEMATICS 2025;6:185–194

ORIGINAL STUDY

Image Denoising: Smooth Total Variation Minimization for 5G Enhanced Mobile Broadband Transmission System

Shehab Ahmed Ibrahem [a], **Walled Khalid Abdulwahab** [a,*], **Moceheb Lazam Shuwandy** [b]

[a] Computer Science Department/University of Kirkuk, Iraq
[b] Computer Science Department/Tikrit Universit, Tikrit, Iraq

ABSTRACT

Image denoising is an important area of computer vision. Rudin-Osher-Fatemi model based on a gradient is one of the simplest models used in image denoising to solve the problem of restoring the clear image. The challenge in solving this model is the non-differentiability of Total Variation function (TV-function) minimization. Image transmission is widespread over wireless systems, including the fifth generation (5G) cellular network. Transmission impairment can affect transmitted images, including noise, attenuation, and distortion. This study proposed a new smoothing technique to make the TV-function differentiable and smooth. The new smoothed function was used for de-noising images with the help of the gradient descent method in minimization. Two transmission systems were proposed, additive white Gaussian noise (AWGN) and 5G enhanced mobile broadband (eMBB), to evaluate the performance of the proposed approach. The denoising technique proved convincing over AWGN and 5G eMBB channel models, reducing the noise effect on the transmitted images. Compared with the noisy image, the gains achieved by the denoised image reached 7.4 and 4174.1 for peak signal-to-noise ratio and mean square error, respectively. These gains are achieved at the low and moderate signal-to-noise ratio regions, while at the high signal-to-noise region, the quality of the noisy and denoised images is almost the same.

Keywords: Total variation, Smoothing function, Image denoising, 5G eMBB, mmWave

1. Introduction

The beginning of the fifth generation (5G) of the digital cellular system was in 2015 [1]. 5G provides new types of services and applications not supported by the previous cellular systems [1, 2]. The fifth mobile generation introduces three use cases which are Enhanced Mobile Broadband (eMBB), Massive Machine Type Communications (mMTC), and Ultra Reliable Low Latency Communications (URLLC). Further, 5G is the first cellular system that uses a new band of spectrum called millimetre waves (mmWaves) in addition to the use of a multi-input multi-output (MIMO) antenna [1, 3]. The eMBB use case, which was deployed in 2019, provided a variety of applications and services to end users with less latency and a lower error rate than 4G, so eMBB is considered an evolution of 4G. Like the previous ones, this cellular network transmits all forms of data, including images. The last one may suffer from distortion during transmission over a wireless channel because of noise, fading, multi path propagation, interference, and other transmission impairments. Image denoising is a crucial field in which many applications deal with image transmission that somehow needs to recover the original image and reduce the noise effect [2, 4].

Received 1 November 2024; revised 22 January 2025; accepted 25 January 2025.
Available online 27 March 2025

* Corresponding author.
E-mail addresses: mullaiq@uokirkuk.edu.iq (S. A. Ibrahem), walled.khalid@uokirkuk.edu.iq (W. K. Abdulwahab), moceheb@tu.edu.iq (M. L. Shuwandy).

https://doi.org/10.52866/2788-7421.1244

In this paper, we consider all images to be in size $n * n$. Let $x^{'} \in \Omega \in R^{n^2}$ be the original image, and let $\omega \in \Omega$ be Gaussian noise. A degraded image $y \in \Omega$ characterized as follows.

$$y = x^{'} + \omega \tag{1}$$

To improve the image and remove noise, this can be solved by taking the inverse of the model Eq. (1), taking into account that regularization techniques try to combine both data-fidelity terms and the model presented in Eq. (1), and put them in the appropriate objective function, and considering the solution to this function as a minimization problem, which is described as follows

$$\min_{f} \{\| f - y \| + \lambda J(f)\} \tag{2}$$

where $J(f)$ is the regularization term and the positive number λ is an equalizer between the two terms in the model Eq. (2). We must choose the appropriate mathematical model for the proposed image to obtain good and accurate results. There are many different mathematical models for describing digital images [4–6]. The total Variation function model (TV function) is an important and effective model for describing digital images because of its capacity to restore the image's edges and preserve its texture very efficiently. The TV function model was first introduced by researchers [7] as a regularizer to reduce image noise, and was later developed and used for denosing [8], and segmentation [9, 10]. So the model in Eq. (2) can be reformulated based on the TV function as follows:

$$\min_{f} \{\|f - y\|_2^2 + \lambda J_{TV}(f)\} \tag{3}$$

where $J_{TV}(f) = \|\nabla f\|_1 = \int_{\Omega} |\nabla f| d\Omega$ represent the TV function, y is a degraded image and f is the image we want to obtain after processing. The model, defined in Eq. (3), contains the TV function, and this function is convex, which indicates that the minimizer is unique. On the other hand, as we mentioned previously, this model is good and effective for removing image noise. Still, there is a problem with the TV function as it is not differentiable due to the presence of the norm term, which is difficult to minimize, and its gradient flow is not well-defined. This problem prompted many researchers to reformulate the model and find an alternative that can be derived [11, 12]. Many researchers have presented alternatives to solve the problem in model Eq. (3); for more information, see [7, 13]. In this paper, we present a new method to solve the problem in model Eq. (3), and then we minimize the new function using one of the local search methods. The gradient descent method [14, 15] is one of the proposed local methods for image denoising and optimization, which has been used to minimize the new function and obtain a good image. Global smoothing was used to solve the problem of model Eq. (3) and make it differentiable. In general, smoothing techniques can be classified into two categories: local [16, 17] and global [18, 19].

In this study, we introduce a new global technique to make TV-function differentiable, and then we use it to denoise the received images in a 5G eMBB transmission system. The structure of this document is as follows: in Section 2, several relevant works are provided. Section 3 defines our study and explains our problem's mathematical solution. Section 4 explains how to adapt the results Section 3 to the denoising problem. In Section 5, additive white Gaussian noise (AWGN) and 5G channel models are presented. The simulation results were shown and discussed in Section 6. Lastly, the conclusion was given in Section 7.

2. Literature survey

Image denoising is a critical issue for wireless communication. The images have to be delivered to the receiver with minimum noise effects. Many studies presented in the literature are concerned with this topic.

In [20] a 34-layer hybrid convolutional neural network (HCNN) scheme was proposed to denoise complex images and overcome the poor performance of the single deep CNN. The HCNN combines several blocks including a single convolution, RepVGG block, dilated block, and feature refinement block. The proposed scheme provided good performance for image and blind denoising. A multi-stage wavelet transformation with convolutional neural network image denoising was proposed in [21], including three stages: enhancement blocks, cascaded wavelet transform, and enhancement blocks. The proposed system outperforms several widespread denoising methods in terms of qualitative and quantitative. In [22] a dual-tree complex wavelet transform was utilized along with the bio-inspired optimization process and artificial neural network to introduce a technique for image denoising. This approach divided the noise into bands by wavelet transform. Then, wavelet-free coefficients were provided by using the neural network. Finally, an optimization algorithm was used to threshold the wavelet coefficients. The introduced scheme provided better performance than other classical methods.

A hyperspectral image denoising model was proposed in [23] with hybrid spatial-spectral total variation and tensor decomposition. The correlations among the modes were inspected, and regularization was presented to avoid over-smoothing. The simulation result shows the superior performance of the proposed method. In [24] a model for representing the total variation regularization was introduced by combining high-order total variation with total variation to overcome the staircase artifact problem which may occur during the removal of the mixed Poisson-Gaussian noise. The results exhibit the advantage of the proposed model compared with various state-of-the-art algorithms.

A cross-transformer denoising approach was proposed in [25] with serial, parallel, and residual blocks to produce spotless images for composite scenes. The transformer mechanisms are embedded into the SB and PB to extract complementary salient features to remove noise. Experiments illustrate that this approach is better than some denoising methods in real and synthetic image denoising.

3. Theoretical part

In this paper, we denote L_2-norm (Euclidean norm) by $\|x\| = \sqrt{x^T.x}, x \in R^n$ and L_1-norm on $[a, b]$ as follows [18]:

$$\|C_r\|_{L^1[a,b]} = \int_a^b |C_r(x)|dx$$

where C_r is a continuous function on the interval $[a, b], a, b \in R$.

Definition 1: [18]: If we have the continuous function $h : R^n \to R$. Then the function $\tilde{h} : R^n \times R_+ \to R$ considers a smoothing function of $h(x)$, if $\tilde{h}(., \sigma)$ is continuous and differentiable function in the domain R^n for any fixed σ, and for any $x \in R^n$,

$$\lim_{z \to x, \sigma \to 0} \tilde{h}(z, \sigma) = h(x).$$

In this section, we suggest a new approach for creating the TV-function differentiable as follows: let $\|u\| = \|\nabla f\|$ and we rewrite the term $|u|$ in one dimension as follows:

$$\phi(u) = |u| = 2uS(u) - u \tag{4}$$

where the function $S : R \to R$ is defined by

$$S(u) = \begin{cases} 1, & u \geq 0, \\ 0, & u < 0. \end{cases}$$

As explained above, the function $S(u)$ is non-smooth, and as a result, $\phi(u)$ is also non-smooth that mean when $S(u) = 1$ the function $\phi(u) = u$ and if $S(u) = 0$ the function $\phi(u) = -u$. Therefore, as we know the function $\phi(u)$ is not smooth, to solve this problem and make the function $\phi(u)$ smooth, it is enough to try to find an alternative to the function $S(u)$ and make it smooth. In this section, we present a new global smoothing technique and an alternative to the $S(u)$ function. In fact, any smoothing function $\tilde{S}_\sigma(u)$ can be used as an alternative to $S(u)$ taking into account the following properties:

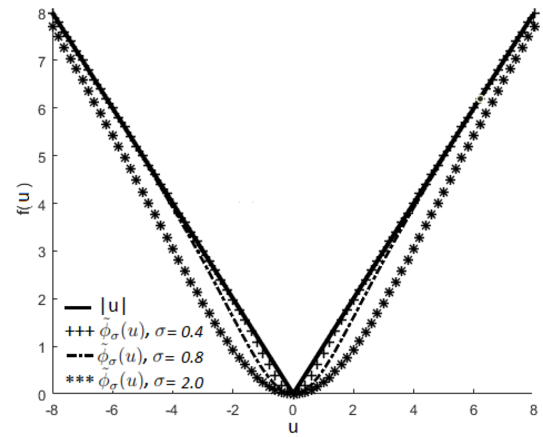

Fig. 1. The functions $\phi(u)$ and $\tilde{\phi}_\sigma(u)$ with deferent values of σ.

. $\lim_{u \to \infty} \tilde{S}_\sigma(u) = 1$,
. $\lim_{u \to -\infty} \tilde{S}_\sigma(u) = 0$,
. $\forall u \in R, \quad \tilde{S}'_\sigma(u) > 0$,
. $\forall u \in (-\infty, 0), \tilde{S}''_\sigma(u) < 0$ and $\forall u \in [0, \infty), \tilde{S}''_\sigma(u) \geq 0$.

Concerning our methodology, we suggest the following smoothing function

$$\tilde{S}_\sigma(u) = \frac{1}{1 + e^{\frac{-u}{\sigma}}} \tag{5}$$

where $\sigma \geq 0$ is a smoothing parameter. It is clearly,

$$\lim_{\sigma \to 0} \tilde{S}_\sigma(u) = \begin{cases} 1 & u > 0, \\ \frac{1}{2} & u = 0, \\ 0 & u < 0. \end{cases} \tag{6}$$

The parameter σ has a major role in controlling the function $\tilde{S}_\sigma(u)$ as it is used to squeeze the function $\tilde{S}_\sigma(u)$ to be asymptotic to the function $S(u)$, which means when $\sigma \to 0$, then the function $\tilde{S}_\sigma(u) \to S(u)$. Finally, we obtain the smoothing version for the function $\phi(u)$ by using Eq. (5) instead of $S(u)$ as follows:

$$\tilde{\phi}_\sigma(u) = 2u\tilde{S}_\sigma(u) - u. \tag{7}$$

and we can see the functions $\phi(u)$ and $\tilde{\phi}_\sigma(u)$ with deferent values of σ in Fig. 1. Based on the above features of the function $\tilde{S}_\sigma(u)$ we introduce the following outcomes.

Theorem 1: *Suppose the functions $\tilde{S}_\sigma(u)$ and $S(u)$ are defined in Eqs. (4) and (5), then for any $\sigma > 0$*

$$\|\tilde{S}_\sigma(u) - S(u)\|_{L^1} \leq \frac{1.39}{\sigma}.$$

Proof. Since we have $u \in (-\infty, \infty)$ then

$$\begin{aligned}\|\tilde{S}_\sigma(u) - S(u)\|_{L^1} &= \int_{-\infty}^{\infty} |\tilde{S}_\sigma(u) - S(u)| d(u) \\ &= \int_{-\infty}^{0} |\tilde{S}_\sigma(u) - (0)| d(u) \\ &\quad + \int_{0}^{\infty} |\tilde{S}_\sigma(u) - 1| d(u) \\ &\leq \frac{1.39}{\sigma}.\end{aligned}$$

Theorem 2: *If the function $\tilde{\phi}_\sigma(u)$ is a smoothing function of $\phi(u)$, then*

$$\|\tilde{\phi}_\sigma(u) - \phi(u)\|_{L^1} \leq \frac{1.65}{\sigma^2}.$$

Proof. We have

$$\begin{aligned}\|\tilde{\phi}_\sigma(u) - \phi(u)\|_{L^1} &= \int_{-\infty}^{\infty} |\tilde{\phi}_\sigma(u) - \phi(u)| du \\ &= 2\int_{-\infty}^{\infty} |u(\tilde{S}_\sigma(u) - S(u))| d(u) \\ &= 2\int_{-\infty}^{0} |u(\tilde{S}_\sigma(u) - (0))| d(u) \\ &\quad + 2\int_{0}^{\infty} |u(\tilde{S}_\sigma(u) - 1)| d(u) \\ &\leq \frac{1.65}{\sigma^2}.\end{aligned}$$

Theorem 3: *Assume that $\tilde{\phi}_\sigma(u)$ is a smoothing function of $\phi(u)$, then*

$$\lim_{\sigma \to \infty} \tilde{\phi}_\sigma(u) = \phi(u).$$

Proof. Since the function $\tilde{S}_\sigma(u)$ is smooth, then the function $\tilde{\phi}_\sigma(u)$ in Eq. (7) should also be defined as a smooth for any $\sigma > 0$. From the Theorem 1, it can be obviously recognized that $\tilde{\phi}_\sigma(u)$ approaches to $\phi(u)$ when $\sigma \to \infty$.

4. Denoising using modified total variation

We employ the rustles from the previous section in this one to make the TV-function smooth. As we mentioned before, we have

$$J_{TV}(f) = \|\nabla f\|$$

and this function's gradient can be computed as

$$\nabla J_{TV}(f) = div\left(\frac{\nabla f}{\|\nabla f\|}\right).$$

The gradient of the TV-function is not defined if at a pixel x one has $f(x) = 0$. This means the TV-function is difficult to minimize, and its gradient flow is poorly defined. To overcome this problem, we consider that instead, a smooth TV-function

$$J_{TV}^{\sigma}(f) = 2\nabla f \tilde{\varphi}(\nabla f) - \nabla f \tag{8}$$

and

$$\tilde{\varphi}(\nabla f) = \frac{1}{1 + e^{\frac{-\nabla f}{\sigma}}}$$

where $\sigma > 0$ is a parameter. Now, the problem which was defined in Eq. (3) can be reformulated based on smoothed TV-function as

$$\min_{f}\{\|f - y\|_2^2 + \lambda J_{TV}^{\sigma}(f)\} \tag{9}$$

We can obtain a good solution for image denoising by using Eq. (9) with the assistance of a gradient descent minimization method, as described in the next algorithm.

5. Channel model

Two transmission system models were proposed to evaluate the submitted image denoising technique. The first transmission system is based on an AWGN channel with a binary phase shift keying (BPSK) as a modulation scheme [26], while the second transmission system is based on a 5G eMMB environment. The last model includes the following components:

1. LDPC encoder/decoder is used for channel coding with a message length 3832 and a coding rate 1/3. This code is supported with the Cyclic Redundancy Code (CRC) for superior performance. The maximum number of iterations used in the LDPC decoder is 8 [27, 28].
2. Quadrature Phase Shift Keying (QPSK) is employed for signal modulation and demodulation to achieve spectral efficiency [29, 30].
3. Orthogonal frequency division multiplexing (OFDM) with a length of 2048 and cyclic prefix

Algorithm

Step1. Locate $k = 0$, given $\sigma > 0, \lambda > 0, \varepsilon > 0$ as a stopping condition, and $\tau > 0$ as a step.
Step2. Suppose $f_0 = y$, where y is a degraded image.
Step3. Find a new solution $f^{(k)+1}$ as follows

$$f^{(k)+1} = f_0 - \tau(f_0 - y + \lambda \nabla J_{TV}^{\sigma}(f_0)).$$

Step4. If $\|f^{(k)+1} - f_0\| > \varepsilon$ then take $f_0 = f^{(k)+1}$, set $k = k + 1$ and goto (Step3); else stop the algorithm and goto (Step5).
Step5. Take $f^{(k)+1}$ as the best solution of image denoising operations.

of length 144 with a subcarrier spacing of 120 KHz is utilized for signal mapping [31, 32].

4. A multiple-input and multiple-output (MIMO) antenna with a dimensionality of 4×4 is applied using Space-Time Block Coding (STBC) [29, 30].
5. A fading channel model approved by 3GPP with a 5G environment is considered. This channel has a maximum bandwidth of 2 GHz and is defined over a frequency range between 0.5 and 100 GHz. This channel model is the tapped delay line E-channel for the umi-street canyon. The proposed channel includes three taps at a carrier frequency of 39 GHz. This frequency lies within the (mmWave) spectrum. The path gains are [−0.03 −15.8 −18.1] in dB. The normalized delays for the taps are [0 0.5133 0.5440] with a delay spread of 30 ns. The K-factor used with this model is 22 dB [33]. A maximum Doppler shift of 77.784 Hz is considered for 3 Km/Hr relative velocity between the transmitting and receiving nodes. The bandwidth of the proposed channel is 200 MHz [31, 34].

6. Simulation result and discussion

In this part, three standard images with a size of 256*256 pixels were used to assess the effectiveness of the suggested denoising approach to minimize the effect of noise on images. These images are the “pepper image”, the “camera-man image”, and the “Lena image”. The Matlab R2021of version (9.10) was used to implement and simulate the proposed system. Two transmission systems, illustrated in Section 5, were utilized to evaluate the image-denoising technique. The simulation results and the discussion of these results are presented in this section.

Two metrics are used to evaluate the performance of the proposed systems which are Peak Signal-to-Noise Ratio (PSNR) and Mean Esquire Error (MSE). PSNR is an evaluation metric widely used to determine the ratio between image and noise power. PSNR can be presented mathematically according to the following equation [20]:

$$PSNR = 10 \times \log_{10}\left(\frac{MAX_I^2}{MSE}\right) \tag{10}$$

MAX represents the maximum value for an image pixel, and MSE is the mean esquire error. MSE represents the mean esquire difference between the original and the reassembled images. The mathematical formula of MSE can be found in the equation below [21]:

$$MSE = \frac{1}{M \times N}\sum_{i=1}^{M}\sum_{j=1}^{N}[I(i, j) - K(i, j))]^2 \tag{11}$$

Where I(i,j) and K(i,j) are the pixel intensity for the original and rebuilt images, M and N are the image’s dimensions. As the value of the PSNR gets high this indicates the enhancement in the quality of the reconstruction image and vice versa. As the value of the MSE gets down that indicates the improvement in the quality of the rebuilt image and vice versa. Both of these metrics will be used to evaluate the performance of the proposed system [20, 21].

6.1. Simulation results

For the AWGN channel, a range of signal-to-noise ratio (SNR) between −6 and 14 dB was considered. The results of the peak signal-to-noise ratio (PSNR) of the received noisy and denoised images for the three considered images are shown in Figs. 2 to 4. In addition, the original, the noisy, and the denoised images at an SNR value of 3 dB are shown in Figs. 5 to 7. Subfigures (a), (b), and (c) refer to the original, noisy, and denoised images, respectively.

The results illustrate that the proposed technique achieved PSNR gains that reached 7.3 dB for the denoised image compared to the noisy one at low and moderate SNR regions for all the considered images. On the other hand, the gains achieved at the high SNR region were reduced. Further, the PSNR for the

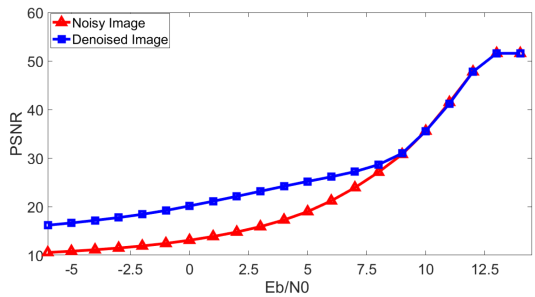

Fig. 2. PSNR for pepper image over AWGN channel.

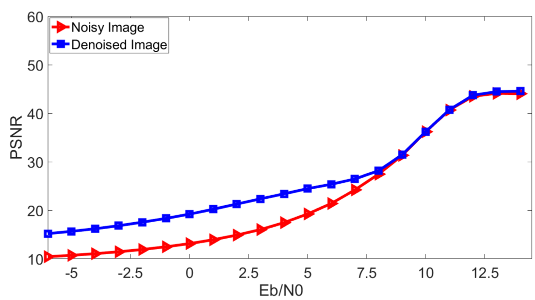

Fig. 3. PSNR for camera man image over AWGN channel.

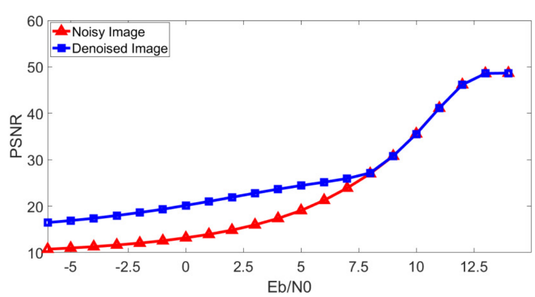

Fig. 4. PSNR for Lena image over AWGN channel.

noisy and the denoised images at the high SNR region became almost identical.

An SNR range from −6 to 1 dB was considered in the simulation over the 5G eMBB transmission system. The PSNR results for the noisy and denoised received images are displayed in Figs. 8 to 10. Further, the original, the noisy, and the denoised samples for the considered images at −2 dB are illustrated in Figs. 11 to 13. The subfigures (a), (b), and (c) in the former figures refer to the original, noisy, and denoised images, respectively.

According to the figures above, the denoised image achieved gains reaching up to 7.4 dB compared to the noisy one in low and moderate SNR ranges (i.e., between −6 and −1) and in all considered cases. At the SNR value of −1 dB, the achieved PSNR gain began to reduce. After this SNR value, the PSNR values for noisy and denoised images become much closer.

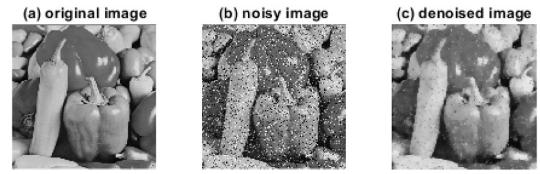

Fig. 5. Pepper image over AWGN channel at 3dB.

Fig. 6. Camera man over AWGN channel at 3dB.

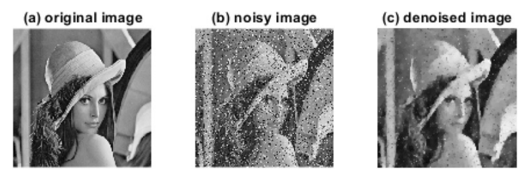

Fig. 7. Lena over AWGN channel at 3dB.

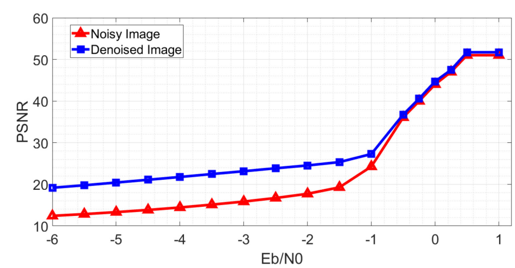

Fig. 8. PSNR for pepper image over 5G eMBB channel.

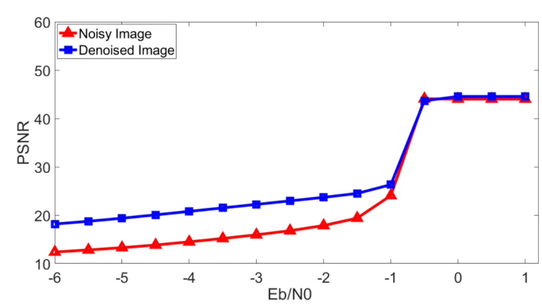

Fig. 9. PSNR for camera man image over 5G eMBB channel.

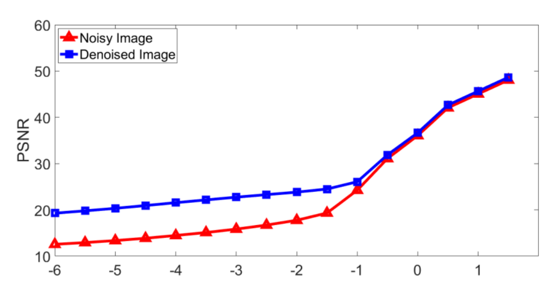

Fig. 10. PSNR for Lena image over 5G eMBB channel.

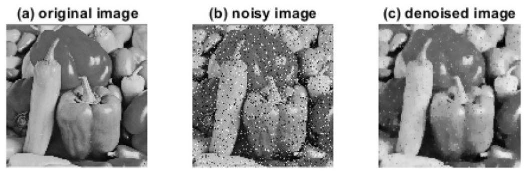

Fig. 11. Pepper image over 5G eMBB channel at −2 dB.

Fig. 12. Camera man image over 5G eMBB.

Fig. 13. Lena image over 5G eMBB channel at −2 dB.

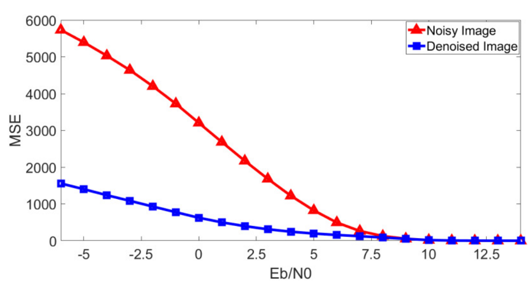

Fig. 14. MSE for pepper image over AWGN channel.

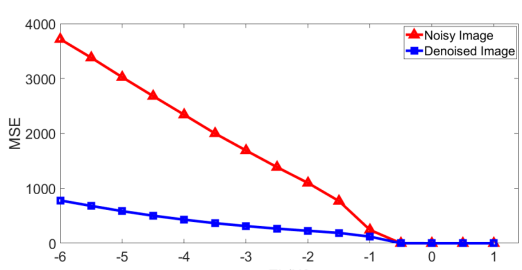

Fig. 15. MSE for pepper image over 5G eMBB channel.

Further evaluation of the proposed model utilizes another metric: the mean square error (MSE). While the PSNR results for the evaluated images are closed over the same channel, only one image, the Pepper image, is considered for evaluating the proposed system based on the MSE metric.

Figs. 14 and 15 present the MSE for the noisy and denoised Pepper image over AWGN and 5G channels, respectively. SNR ranges of −6 to 14 and −6 to 1 are considered over AWGN and 5G channels, respectively.

According to these figures, the denoised images achieved high reductions in MSE compared with noisy images at low and moderate SNR reaching up to 4174 and 2937 over AWGN and 5G channels, respectively. The MSE for both noisy and denoised images at high SNR values becomes closed over both channels.

6.2. Result discussion

The proposed denoising technique performs well in minimizing the effect of noise on the received images. In addition to the theoretical proofs for the denoising technique in sections 3 and 4, the evaluation of the proposed system showed that the denoised images achieved gains in terms of PSNR and MSE over the noisy ones and for all considered cases. This gain was between 0 and 7.4 dB for PSNR and between 0 and 4174 for MSE. Tables 1 and 2 present the details of the PSNR gain provided by the denoising system over the AWGN and 5G channels, respectively. Tables 3 and 4 show the details of the MSE reduction provided by the denoising system over the AWGN and 5G channels, respectively.

According to Table 1, the PSNR for the noisy image increased from 10.5, 10.4, and 10.7 dB at an Eb/No of −6 dB to 51.6, 44, and 48.6 at an Eb/No value of 14 dB for pepper, camera man, and Lina Image, respectively. On the other hand, the PSNR for the denoised images increased from 16.2, 15.2, and 16.5 to 51.6, 44,6, and 48.6 over the same Eb/No range for pepper, camera man, and Lina Images, respectively. Thus, the PSNR gains achieved by the denoised pepper image over the noisy one are distributed between 0 and 7.3 dB over the SNR range −6 and 14 dB.

For Table 2, the PSNR for the noisy pepper, camera man, and Lina images increased from 12.4, 12.4, and 12.5 dB to 51, 44, and 45 dB, respectively, over the evaluated Eb/No range between −6 and 1 dB. Furthermore, the PSNR for the denoised image enhanced from 19.2, 18.2, and 19.3 to 51.7, 44.6, and 45.6 dB for pepper, camera man, and Lina images, respectively, and over the same Eb/No values. Consequently, the achieved gains varied between 0.6 and 6.3 over the SNR range −6 and 1 dB.

Related to Table 3, the MSE for the noisy image reduced from 5732.5 at an Eb/No of −6 dB to 0 at an Eb/No value of 13 dB for the pepper image. Conversely, the MSE for the denoised images reduced from 1558.4 to 0 over the same Eb/No range for the pepper Image. Thus, the MSE gains achieved by the denoised pepper image over the noisy one are

Table 1. PSNR for noisy and denoised images and PSNR gain over AWGN channel.

	PSNR forNoisy Image [dB]			PSNR for Denoised Image [dB]			PSNR Gains [dB]		
SNR Value [dB]	Pepper Image	Camera Man Image	Lena Image	Pepper Image	Camera Man Image	Lena Image	Pepper Image	Camera Man Image	Lena Image
−6	10.5	10.4	10.7	16.2	15.2	16.5	5.7	4.8	5.8
−4	11.1	11	11.3	17.2	16.2	17.4	6.1	5.2	6.1
−2	11.9	11.9	12	18.4	17.5	18.6	6.5	5.6	6.6
0	13	13.1	13.2	20.1	19.2	20.1	7.1	6.1	6.9
2	14.8	14.9	14.8	22.1	21.3	21.9	7.3	6.4	7.1
4	17.3	17.7	17.3	24.2	23.4	23.7	6.9	5.7	6.4
6	21.2	21.4	21.3	26.1	25.4	25.2	4.9	4	3.9
8	27.1	27.4	27	28.6	28.1	27.5	1.5	0.7	0.5
10	35.6	36.2	35.6	35.6	36.2	35.6	0	0	0
12	47.8	43.5	46.1	47.8	43.7	46.1	0	0.2	0
14	51.6	44	48.6	51.6	44.6	48.6	0	0.6	0

Table 2. PSNR for noisy and denoised images and PSNR gain over 5G eMBB transmission.

	PSNR forNoisy Image [dB]			PSNR for Denoised Image [dB]			PSNR Gains [dB]		
SNR Value [dB]	Pepper Image	Camera Man Image	Lena Image	Pepper Image	Camera Man Image	Lena Image	Pepper Image	Camera Man Image	Lena Image
−6	12.4	12.4	12.5	19.2	18.2	19.3	6.8	5.8	6.8
−5	13.3	13.3	13.4	20.4	19.5	20.3	7.1	6.2	6.9
−4	14.4	14.5	14.5	21.8	20.8	21.5	7.4	6.3	7
−3	15.9	16	15.8	23.1	22.2	22.7	7.2	6.2	6.9
−2	17.7	17.9	17.7	24.5	23.7	23.8	6.8	5.8	6.1
−1	24.3	24	24.2	27.3	26.3	26.1	3	2.3	1.9
0	44	44	36	44.7	44.6	36.6	0.7	0.6	0.6
1	51	44	45	51.7	44.6	45.6	0.7	0.6	0.6

Table 3. MSE for noisy and denoised images and MSE reduction over AWGN channel.

SNR [dB]	MSE Noisy	MSN De-noisy	Reduction in MSE
−6	5732.5	1558.4	4174.1
−5	5395.5	1400.6	3994.9
−4	5031.4	1239.1	3792.3
−3	4640.1	1085.2	3554.9
−2	4201.3	930.2	3271.1
−1	3725.3	775.5	2949.8
0	3204.5	625	2579.5
1	2684.3	500.2	2184.1
2	2171.5	396.4	1775.1
3	1682	311.9	1370.1
4	1222.9	245.9	977
5	824.3	195.7	628.6
6	494.9	157	337.9
7	264.5	123.1	141.4
8	127.1	88.3	38.8
9	54.5	51.6	2.9
10	17.9	17.7	0.2
11	4.7	4.6	0.1
12	0.8	0.7	0.1
13	0	0	0
14	0	0	0

distributed between 0 and 4174.1 over the SNR range −6 and 14 dB.

For Table 4, the MSE for the noisy pepper image reduced from 3717.0 to 0 over the evaluated Eb/No range between −6 and 1 dB. Furthermore, the MSE for the denoised image reduced from 779.8 to 0 for the pepper image over the same Eb/No values. Consequently, the achieved gains varied between 0 and 2937.2 over the SNR range −6 and 1 dB.

Table 4. MSE for noisy and denoised images and MSE reduction over 5G channel.

SNR [dB]	MSE for Noisy Image	MSE for Denoised Image	Reduction in MSE
−6	3717.0	779.8	2937.2
−5.5	3379.5	680.2	2699.3
−5	3024.6	584.9	2439.7
−4.5	2680.2	501.6	2178.6
−4	2341.0	429.9	1911.1
−3.5	1999.7	365.3	1634.4
−3	1689.5	312.8	1376.6
−2.5	1385.6	265.6	1120
−2	1097.8	227.2	870.6
−1.5	768.4	188.7	579.7
−1	243.1	120.7	122.4
−0.5	0.3	0.2	0.1
0	0	0	0
0.5	0	0	0
1	0	0	0

The PSNR gains achieved for the tested images over the AWGN channel and 5G eMBB transmission system are shown in Figs. 16 and 17, respectively. Related to the AWGN channel case, the peak value of PSNR gain was achieved at an Eb/No value of 2 dB. Further, the

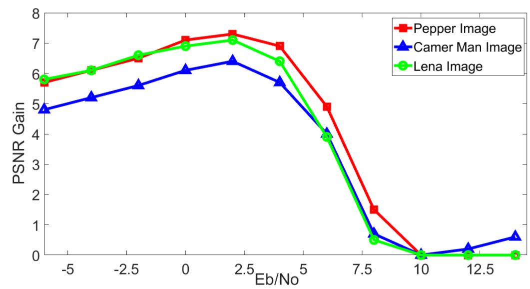

Fig. 16. PSNR gain for AWGN channel.

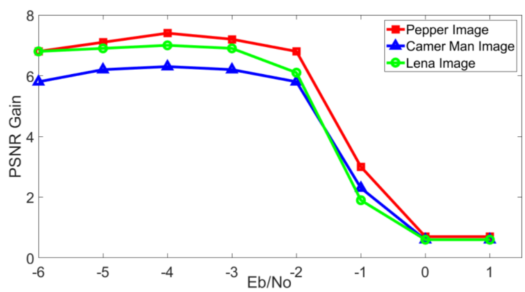

Fig. 17. PSNR gain for 5G eMBB channel.

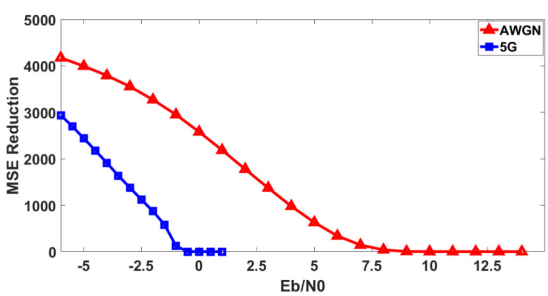

Fig. 18. MSE reduction for AWGN and 5G eMBB channels.

highest PSNR gains were realized over the range of Eb/No between −6 and 5 dB. Before 6 dB, the PSNR gains were reduced and reached zero at 10 dB.

Fig. 18 shows the reduction in MSE achieved for the tested image over the AWGN channel and 5G eMBB transmission system. For the considered case, the maximum gains were achieved at low and moderate SNR values, while at the high SNR region, the MSE gain reduced until reaching 0.

For the 5G eMBB case, the peak PSNR values attained at Eb/No value of −4 dB. The highest PSNR gains were reached at the Eb/No domain between −6 and −2. After that, the PSNR gains were brought down to values below 1 dB at Eb/No of 0 dB.

Consequently, the proposed approach in image denoising enhanced the quality of the denoised images compared with the noisy ones. Furthermore, the effective regions of the denoising approach are the low and moderate SNR regions.

7. Conclusions

This paper introduced a new smoothing technique to minimize the noise effect on images transmitted over a 5G eMBB transmission system using a mathematical model based on TV function. The last function was modified to be differentiable and smooth. It was proved to be effective in image denoising capability. In addition, two-channel models were proposed; the first model is an ideal channel, i.e., Additive White Gaussian Noise channel, while the second model simulates a real modern channel model. The last one is based on the parameters of the fifth generation of mobile communication standards. The performance of the proposed smoothing technique was evaluated over these channel models, and it showed persuasive behavior. The denoised image provided gains in PSNR and MSE over the noisy ones at low and moderate SNR regions.

References

1. P. Marsch, Ö. Bulakci, O. Queseth, and M. Boldi, “5G system design: Architectural and functional considerations and long term research,” John Wiley & Sons, 2018.
2. H. Kim, “Design and optimization for 5G wireless communications,” John Wiley & Sons, 2020.
3. A. F. Molisch, “Wireless communications: From fundamentals to beyond 5G,” John Wiley & Sons, 2022.
4. A. M. Bruckstein, D. L. Donoho, and M. Elad, “From sparse solutions of systems of equations to sparse modeling of signals and images,” *SIAM review*, vol. 51, no. 1, pp. 34–81, 2009.
5. L. Ao, L. Yibing, Y. Xiaodong, and L. Yue, “Image restoration with dual-prior constraint models based on split bregman,” *Optical Review*, vol. 20, pp. 491–495, 2013.
6. D. L. Phillips, “A technique for the numerical solution of certain integral equations of the first kind,” *Journal of the ACM (JACM)*, vol. 9, no. 1, pp. 84–97, 1962.
7. L. I. Rudin and S. Osher, “Total variation based image restoration with free local constraints,” In *Proceedings of 1st international conference on image processing*, vol. 1, pp. 31–35, 1994.
8. A. Beck and M. Teboulle, “Fast gradient-based algorithms for constrained total variation image denoising and deblurring problems,” *IEEE transactions on image processing*, vol. 18, no. 11, pp. 2419–2434, 2009.
9. Y. He, M. Y. Hussaini, J. Ma, B. Shafei, and G. Steidl, “A new fuzzy c-means method with total variation regularization for segmentation of images with noisy and incomplete data,” *Pattern Recognition*, vol. 45, no. 9, pp. 3463–3471, 2012.
10. T. F. Chan, S. Esedoglu, and M. Nikolova, “Algorithms for finding global minimizers of image segmentation and denoising models,” *SIAM journal on applied mathematics*, vol. 66, no. 5, pp. 1632–1648, 2006.
11. A. Chambolle, “Total variation minimization and a class of binary mrf models,” In *International Workshop on*

Energy Minimization Methods in Computer Vision and Pattern Recognition. Springer, 2005, pp. 136–152.
12. T. F. Chan, G. H. Golub, and P. Mulet, “A nonlinear primal-dual method for total variation-based image restoration,” *SIAM journal on scientific computing*, vol. 20, no. 6, pp. 1964–1977, 1999.
13. A. Marquina and S. Osher, “Explicit algorithms for a new time dependent model based on level set motion for nonlinear deblurring and noise removal,” *SIAM Journal on Scientific Computing*, vol. 22, no. 2, pp. 387–405, 2000.
14. A. Chambolle, “An algorithm for total variation minimization and applications,” *Journal of Mathematical imaging and vision*, vol. 20, pp. 89–97, 2004.
15. J. Yang, W. Yin, Y. Zhang, and Y. Wang, “A fast algorithm for edge-preserving variational multichannel image restoration,” *SIAM Journal on Imaging Sciences*, vol. 2, no. 2, pp. 569–592, 2009.
16. D. P. Bertsekas, “Nondifferentiable optimization via approximation,” In *Nondifferentiable optimization*. Springer, 2009, pp. 1–25.
17. N. Yilmaz and A. Sahiner, “New smoothing approximations to piecewise smooth functions and applications,” *Numerical Functional Analysis and Optimization*, vol. 40, no. 5, pp. 513–534, 2019.
18. A. Sahiner and S. A. Ibrahem, “A new global optimization technique by auxiliary function method in a directional search,” *Optimization Letters*, vol. 13, pp. 309–323, 2019.
19. Y. Xiao and B. Yu, “A truncated aggregate smoothing newton method for minimax problems,” *Applied Mathematics and Computation*, vol. 216, no. 6, pp. 1868–1879, 2010.
20. M. Zheng, K. Zhi, J. Zeng, C. Tian, and L. You, “A hybrid cnn for image denoising,” *Journal of Artificial Intelligence and Technology*, vol. 2, no. 3, pp. 93–99, 2022.
21. A. Jameel Naji, S. A Ibrahem, and S. U Umar, “Improved image segmentation method based on optimized higher-order polynomial,” *International Journal of Nonlinear Analysis and Applications*, vol. 14, no. 1, pp. 2701–2715, 2023.
22. M. Rmaidh and S. Ibrahim, “A new method for solving image segmentation problems using global optimization,” *International Journal of Intelligent Systems and Applications in Engineering*, vol. 11, pp. 85–92, 2023.
23. P. Zhang and J. Ning, “Hyperspectral image denoising via group sparsity regularized hybrid spatio-spectral total variation,” *Remote Sensing*, vol. 14, no. 10, p. 2348, 2022.
24. C. T. Pham, T. T. T. Tran, H. V. Dang, and H. P. Dang, “An adaptive image restoration algorithm based on hybrid total variation regularization,” *Turkish Journal of Electrical Engineering and Computer Sciences*, vol. 31, no. 1, pp. 1–16, 2023.
25. C. Tian, M. Zheng, W. Zuo, S. Zhang, Y. Zhang, and C.-W. Lin, “A cross transformer for image denoising,” *Information Fusion*, vol. 102, p. 102043, 2024.
26. M. Forkan, A. Halder, M. N. N. Ripa, and M. R. Tanshen, “Performance analysis of bpsk & 8-fsk modulation technique through awgn channel in wireless communication system,” *AIJR Proceedings*, pp. 52–59, 2022.
27. 3rd Generation Partnership Project, “5g; nr; multiplexing and channel coding,” *TS 38.212 version 17.2.0 Release 17*, 2022.
28. T. T. B. Nguyen, T. Nguyen Tan, and H. Lee, “Efficient qc-ldpc encoder for 5g new radio,” *Electronics*, vol. 8, no. 6, p. 668, 2019.
29. W. K. Abdulwahab and A. A. Kadhim, “Internal pilot insertion for polar codes,” *Indonesian Journal of Electrical Engineering and Computer Science (IJEECS)*, vol. 22, no. 3, pp. 1495–1504, 2021.
30. W. K. Abdulwahab and A. A. Kadhim, “Reduced path successive cancellation list decoding for polar codes.” *International Journal of Engineering & Technology Innovation*, vol. 11, no. 1, 2021.
31. 3rd Generation Partnership Project, “5g; nr; user equipment (ue) radio transmission and reception; part 2: range 2 standalone,” *TS 38.101-2 version 17.6.0 Release 17*, 2022.
32. A. A. Kadhim and W. Abdulwahab, “Scalable video transmission using ofdm schemes over wireless channels,” In *2012 International Conference on Future Communication Networks*. IEEE, 2012, pp. 63–68.
33. 3rd Generation Partnership Project, “5g; study on channel model for frequencies from 0.5 to 100 ghz,” *TR 38.901 version 16.1.0 Release 16*, 2020.
34. 3rd Generation Partnership Project, “5g; nr, base station (bs) conformance testing part1:conduct conformance testing,” *TS 38.141-1 version 16.12.0 Release 16*, 2022.